Available online at www.sciencedirect.com
ScienceDirect
Solid State Sciences 9 (2007) 394–403
www.elsevier.com/locate/ssscie

Carbonate phobic (Zn,Mn)-Al hydrotalcite-like compounds

Alvaro Sampieri [a,*], Geolar Fetter [b], Heriberto Pfeiffer [a], Pedro Bosch [a]

[a] *Instituto de Investigaciones en Materiales, Universidad Nacional Autónoma de México, A.P. 70360, Ciudad Universitaria, C.P. 04510 México, D.F., Mexico*

[b] *Facultad de Ciencias Químicas, Universidad Autónoma de Puebla, Blvd. 14 Sur y Av. San Claudio, C.P. 72570 Puebla, PUE, Mexico*

Received 9 February 2007; received in revised form 13 March 2007; accepted 15 March 2007
Available online 31 March 2007

Abstract

The synthesis method of three series of nitrated (Zn,Mn)-Al hydrotalcites in the presence of microwave irradiation is presented. MnO_4^- anions were partially incorporated between the layers of those compounds and a staged intercalation occurred. In the presence of CO_2, nitrated and permanganate intercalated hydrotalcites were tested in CO_3^{2-} retention. Carbonate phobic character was observed and it may be correlated to the poor basicity of hydrotalcites, thus, to the electronegativity of M^{2+} cations.

Keywords: Hydrotalcite-like compounds; MnO_4^- incorporation; CO_2 sorption; Electronegativity; Microwave irradiation

1. Introduction

Hydrotalcite-like compounds (HT) are layered double hydroxide minerals. They are natural or synthetic anionic clays with positively charged layers balanced by hydrated anions [1]. HT composition is defined by the general formula $[M^{2+}_{1-x}M^{3+}_x(OH)_2][A^{n-}_{x/n}\cdot mH_2O]$, with $x =$ molar ratio $M^{3+}/(M^{2+}+M^{3+})$ and $0.2 < x < 0.33$. The layer structure is usually constituted by octahedrally coordinated divalent (Mg^{2+}, Ni^{2+}, Zn^{2+}, …) and trivalent (Al^{3+}, Cr^{3+}, …) cations, sharing edges to form infinite brucite-like sheets, $Mg(OH)_2$. The interlayer space may be occupied by CO_3^{2-}, NO_3^-, Cl^-, etc. [1,2] or more complex anions [2] as $Fe(CN)_6^{3-}$, $Fe(CN)_6^{4-}$, $V_2O_7^{6-}$, $Mo_7O_{24}^{6-}$. Hydrotalcites are versatile materials [3] since their properties may be modulated by changing the molar ratio, $M^{3+}/(M^{2+}+M^{3+})$, therefore altering the brucite-like layer charge. Then, the amount and the type of interlayered anions may be controlled.

Hydrotalcites can be synthesized through several precipitation methods [1–6]. Coprecipitation is the usual procedure, it is a time consuming technique, which requires large volumes of water. This method in the presence of microwave irradiation, not only reduces preparation time, but it provides original materials. For instance in Mg/Al hydrotalcite microwave-assisted synthesis, the resulting materials present a concentration gradient where the core is aluminium enriched. This effect may be attributed to the competitive diffusion determined by charge, weight and ion size. As aluminiums are the cations associated with the interlayered anions, they determine the location of those anions, then in the microwave-assisted synthesis they should be located in the core of the particle [7].

The Mg–Al HT preference towards divalent ions is as follows: $SO_4^{2-} < NYS^{2-} < CO_3^{2-}$ and for monovalent anions it is $I^- < NO_3^- < Br^- < Cl^- < F^- < OH^-$ [3,8]. Those sequences depend mainly on aluminium content, anion type, water content and calcination temperature. Carbonates are always preferred and it is a hard task to inhibit the formation of CO_3^{2-} hydrotalcite [9]. If iodine, for example [10], has to be retained, the hydrotalcite must be thermally treated to eliminate carbonates and obtain the metallic oxides which are the precursors to reconstruct HT with iodine as interlayered anion. Therefore, the synthesis of a carbonate phobic hydrotalcite is highly suitable to avoid the calcination step.

* Corresponding author. Tel.: +52 (55) 5622 4641; fax: +52 (55) 5616 1371.
E-mail address: asamcr@yahoo.com (A. Sampieri).

1293-2558/$ - see front matter © 2007 Elsevier Masson SAS. All rights reserved.
doi:10.1016/j.solidstatesciences.2007.03.014

In this work we propose to substitute Mg by Zn or Mn and we study the corresponding performance in carbonate retention. We chose Zn and Mn to modify the polarities in the hydroxide layers. In this sense, the synthesis of nitrated (Zn,Mn)-Al HTs in the presence of microwave irradiation is presented. Then, MnO_4^- and CO_2 were selected to test the obtained nitrated materials. Indeed, MnO_4^- is an anion ($A_{x/n}^{n-}$) and CO_2 is a gas prone to react and forms carbonate anions which may be intercalated.

2. Experimental section

2.1. Hydrotalcites preparation

Binary Zn–Al and Mn–Al HT with a M^{2+}/Al^{3+} molar ratio of 2/1 were synthesized by coprecipitation [11]. Two aqueous solutions, one containing both $Mn(NO_3)_2$ from Aldrich, 98% (or $Zn(NO_3)_2$ from Baker, 99%) and $Al(NO_3)_3$ from Aldrich, 99%, hydrated salts, and the other NaOH (1.85 M) from Baker, 98%, were added dropwise into a flask at room temperature. The pH was maintained between 7.5 and 8.5 to avoid the ZnO formation [12–14]. After precipitation, samples were irradiated in a microwave oven (MIC-I, Sistemas y Equipos de Vidrio, S. A. de C. V.) operating at 200 W for 10 min to accelerate condensation and crystallization steps [7]. The maximal temperature reached into the reactor was 353 K. The mixture final volume was about 400 ml to obtain *ca.* 20 g of dried product. Prior to drying at 343 K for 24 h, the precipitates were washed with deionized water. The nitrated Zn–Al HT was white, while the nitrated Mn–Al sample turned out to be brown. The ternary nitrated (Zn-Mn)-Al HT was synthesized in the same way with a Zn/Mn/Al molar ratio of 0.2/1.8/1.0. An intense brown color was the feature of the dried product. All hydrotalcite-like compounds were calcined at 523 and 723 K in a mufle for 2 h.

2.2. Insertion of MnO_4^-

Two methods were used to introduce the MnO_4^- anions: on the one hand, through anion exchange and on the other, through memory effect. The anion exchange procedure is described in Ref. [15]. Two grams of each nitrated hydrotalcite (before the drying step) were suspended in 200 ml of an aqueous solution of $KMnO_4$ (0.3 M). Anion-exchange reaction was performed while stirring at room temperature. The mixture was then irradiated in a microwave oven (200 W for 10 min). The samples were centrifuged, washed extensively and dried at 343 K. The second procedure to incorporate MnO_4^- into the nitrated HT was *via* the memory effect. An appropriate amount of samples calcined at 523 or 723 K was added to 200 ml of an aqueous solution of $KMnO_4$ (0.3 M). The suspension was stirred and subsequently microwave irradiated at the previous conditions. The resulting product was washed several times, centrifuged and dried at 343 K.

2.3. CO_2 test

The CO_2 effect was followed in the TGA experiments as explained later. These experiments were carried out to determine the CO_2 retention.

As a reference, memory effect efficiency of the calcined NO_3^--HTs was tested by mixing the samples with a Na_2CO_3 aqueous saturated solution and stirring for several days at room temperature. In such conditions, a calcined Mg–Al HT is usually reconstructed [8].

2.4. Characterization

X-ray diffraction (XRD) patterns were recorded with a Bruker axs D8 advance diffractometer coupled to a copper anode X-ray tube. X-ray thermo-diffraction was carried out from 333 to 683 K with a temperature scanning step of 35 K.

N_2 adsorption–desorption isotherms were measured with a Micromeritics ASAP 2020 system at 77 K. Prior to analysis, the samples were pretreated in vacuum at 473 K for 5–6 h. This pretreatment was chosen after the thermo-diffraction and TGA experiments. Total pore volume was evaluated from the desorption branch of the isotherm using the BJH model.

A Perkin–Elmer GX series spectrometer in a wavenumber interval of 4000–400 cm^{-1} was used to measure the FTIR spectra. The DTGS detector had a resolution of 2 cm^{-1}. The powder samples were not diluted.

Scanning electron microscopy (SEM) images were recorded with a Cambridge Leica Stereoscan 440 microscope. Samples were previously coated with gold to avoid the lack of conductivity. X-ray energy dispersive analysis (EDX) system was coupled to the SEM.

TGA-N_2 and CO_2 experiments were carried out from room temperature to 1273 or 1173 K at the rate of 10 K min^{-1}, with a TA Instruments equipment. CO_2 sorption experiments were analyzed using the same TGA instrument. A total of 50 mg of HT were pretreated in N_2 from room temperature to 423 K (5 K min^{-1}). The sorption step was then performed isothermally (at 423 K) under gas flow (60 ml min^{-1}) of carbon dioxide for 2 h.

3. Results

3.1. Dried nitrated samples

3.1.1. X-ray diffraction

The XRD patterns of the HTs dried at 343 K are shown in Fig. 1. They all correspond to a hydrotalcite-like structure, the average d_{003} distance is 8.846 Å for the three samples; the d_{003} distance is similar to the often reported value in nitrated HTs [8]. Thus, the interlayer space is *ca.* 4.0 Å as 4.8 Å is the thickness of the brucite-like layer. Still, a small amount of a spinel appears in the ternary (Zn-Al)-Al HT attributed to the oxidation of the reactants during preparation [16], probably favoured by the microwave irradiation. The brown color of the Mn samples has to be attributed to the

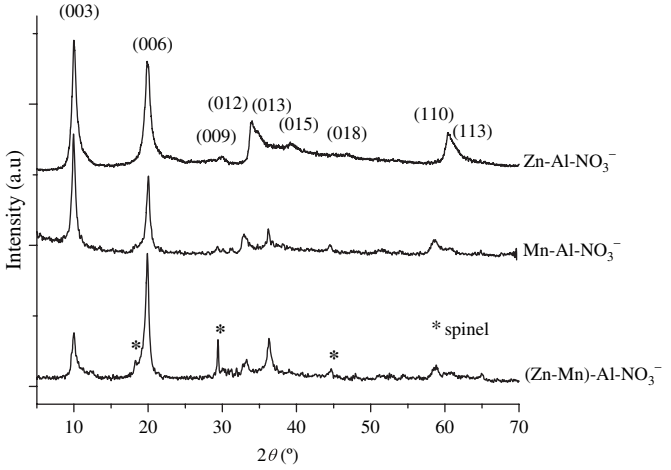

Fig. 1. XRD patterns of nitrated HTs dried at 343 K.

oxidation process: Mn(II) to Mn(IV). Indeed, Mn(II) cations in an octahedral OH environment are slightly pink (as hexa aqueous manganese(II) cations). Nevertheless, these compounds are present in a very low concentration.

Besides, parameters a and c, displayed in Table 1, are consistent with a hexagonal unit cell; they were obtained from the hydrotalcite (110) and (003) reflections, respectively. Cell parameter a is smaller in the Zn−Al HT (3.060 Å) than in the Mn−Al HT (3.153 Å). As Mn^{2+} ionic radius (0.80 Å) is larger than the Zn^{2+} ionic radius (0.74 Å) [1], then Zn^{2+} and Mn^{2+} are inserted in the brucite layers of the corresponding samples. In the ternary material, (Zn-Al)-Al HT, the a parameter is 3.150 Å. This value is larger (0.010 Å) than the value obtained using the Végard law ($a = 3.140$ Å) with the molar nominal composition Zn/Al = 0.2. As spinel precipitated, the HT composition is different, again using the Végard law to determine the Zn/Mn ratio from the cell parameters, the following hydrotalcite composition is obtained, $Zn_{0.06}Mn_{1.94}Al_{1.0}$, which corresponds to a Zn/Al value of 0.06. The nominal composition does not correspond to the formed compounds, as a high amount of Zn did not react and was eliminated during the washing step or was incorporated into the spinel. Furthermore, the determination of the Zn/Al ratio through the Végard law should be more trustable than the ratio obtained through a conventional chemical analysis as it corresponds only to the hydrotalcite and does not incorporate the contribution of the segregated oxides. Lastly, the (006) X-ray diffraction peak intensity is higher than the intensity of the (003) reflection in the (Zn,Mn)-Al-NO_3. To explain such difference, it has been proposed that a heavy metal is located at the midpoint of the interlayer galleries [17,18].

3.1.2. Scanning electron microscopy and EDX analyses

Table 2 compares the M/Al bulk molar ratios obtained by EDX analyses and XRD (Végard law). In the ternary sample Zn/Al = 0.57, value obtained by EDX, showing that the amount of Zn in the HT is higher than the nominal. This result is not in agreement with the XRD measurements. As microscopy is a local analysis and X-ray diffraction corresponds to the bulk of the hydrotalcite sample, the homogeneity of this material is not guaranteed. Furthermore, the EDX analysis may correspond to a spinel particle. Therefore, the probable composition of the spinel is $Zn_{1-x}Al_xMn_2O_4$, where $x \approx 0.57$ corresponding to the Al/Zn spinel ratio. Of course, such information is much richer than the one provided by a conventional elementary analysis, for instance atomic absorption spectroscopy. Indeed, the values reported in this work are selective as they differ between bulk and surface or spinel and hydrotalcite.

Even in low magnification micrographs, the HT morphologies are different (Fig. 2A, C and E). The Zn−Al HT surface is smooth and clean, instead the Mn−Al HT presents small faceted adhered particles. The (Zn-Al)-Al HT is very similar to the Mn−Al HT. If the magnification is higher, these remarks are confirmed. In the Zn−Al sample, grains are shaped as small flakes *ca.* 0.5−1.0 μm (Fig. 2B). This morphology is also present in other preparations, Fig. 2D and F, where the grain sizes (0.5 μm ≤ d ≤ 4 μm) and their distributions are different. Again, the grains in the samples containing Mn^{2+} have a similar morphology.

The homogeneity of metal distribution in the HTs was then established by mapping Zn, Al and Mn elements by EDX. In Zn−Al HT, both elements Zn and Al are homogeneously distributed (Fig. 3A). Instead, in the Mn containing materials (Fig. 3B and C), zones poor in Al and Zn are detected, mainly for the (Zn-Mn)-Al sample. These zones correspond to the manganese oxides reported by XRD or to the Mn surface enriched HT grains.

3.1.3. N_2-TGA experiments

The initial weight loss at 393−423 K is attributed to the removal of interlayered water molecules (Fig. 4); the layered structure is preserved. The HT lattice collapses, between 473 and 783 K, due to the removal of interlayered NO_3^- and hydroxyl groups. The total weight loss was estimated to be

Table 1
Cell parameters obtained by XRD from nitrated HTs dried at 343 K

NO_3^--HT	Dried samples		
	$d_{(003)}$ (Å)	a (Å, ±0.001)	c (Å, ±0.001)
Zn−Al	8.814	3.060	26.441
Mn−Al	8.882	3.153	26.645
(Zn-Mn)-Al	8.841	3.150	26.522

a and c parameters were obtained from $a = 2d_{110}$ and $c = 3d_{003}$. The NaCl was used as internal reference.

Table 2
Comparison of the Zn/Al and Mn/Al molar ratios obtained by XRD and EDX analyses

NO_3^--HT	Zn/Al		Mn/Al	
	XRD	EDX	XRD	EDX
Zn−Al	2.0	2.06	–	–
Mn−Al	–	–	2.0	1.94
(Zn-Mn)-Al	0.06	0.57	1.94	1.46

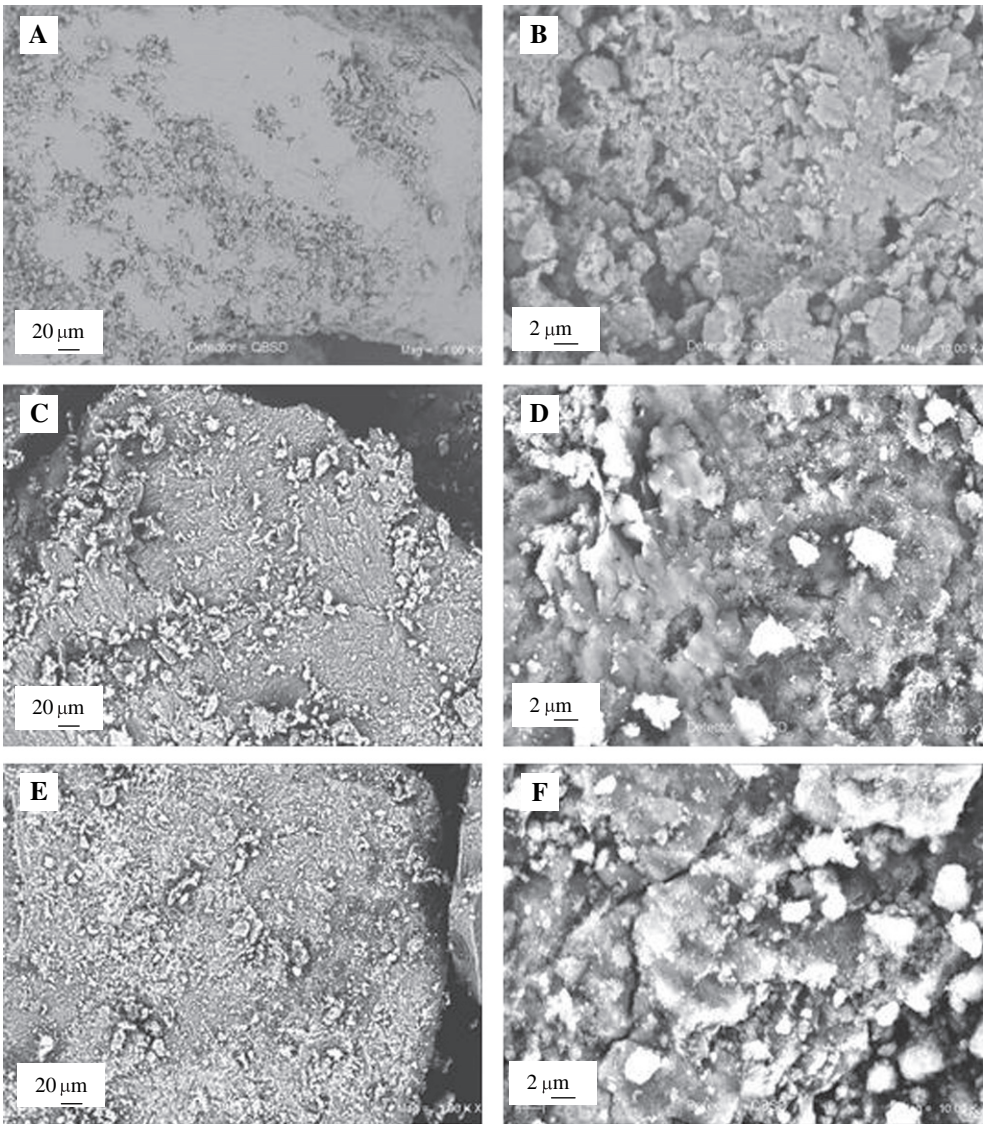

Fig. 2. SEM images from Zn–Al (A, B), Mn–Al (C, D) and (Zn-Mn)-Al (E, F) nitrated HTs.

35 wt% (±2) for the three samples. Again, the ternary preparation behaviour is intermediate between the two binary HTs.

3.1.4. CO_2 sorption

To determine the CO_2 retention efficiency of our materials, TGA curves were obtained in CO_2 atmosphere. If the resulting profiles are compared to those obtained in N_2 atmosphere, no different weight losses are observed (Fig. 5). It has to be underlined that no initial mass uptake is observed under CO_2 atmosphere. Therefore, no CO_2 is retained either as carbon dioxide or carbonate. To be sure that the HT structure was maintained, isothermal TGA experiments were carried out at 423 K (Fig. 6). An initial pretreatment, for 25 min under N_2 current, showed that almost 7–9 wt% was lost. It may be attributed to interlayered water. When the gas flux was CO_2, the Zn–Al HT weight remained constant. Instead the Mn containing samples followed a different trend, they lost *ca*. 6 wt%, also attributed to water. Such different behaviour has to be correlated with the specific surface areas reported previously as well as to the nitrate content. The Mn layered compounds loose water even if the environmental gas is CO_2, showing that water occupies the interlayer space (Fig. 6). Of course, these curves also indicate that the HTs are unable to trap CO_2. A second hypothesis could be that NO_3^- anions are totally exchanged by CO_3^{2-} anions since the beginning of the preparations. This would induce a mass loss of about 12 wt%. However, such proposition has to be discarded as the (Zn-Mn)-Al NO_3^- looses more weight than the Mn–Al NO_3^-. This sample contains a non-negligible fraction of spinel. Furthermore, the nitrates are exchanged by carbonates which are only formed in the presence of water.

3.2. Calcined samples

3.2.1. X-ray diffraction

The binary HTs, Zn–Al and Mn–Al samples, treated at 523 K, Fig. 7, present ZnO, $ZnAl_2O_4$ and/or Mn_2O_4, Mn_2O_3.

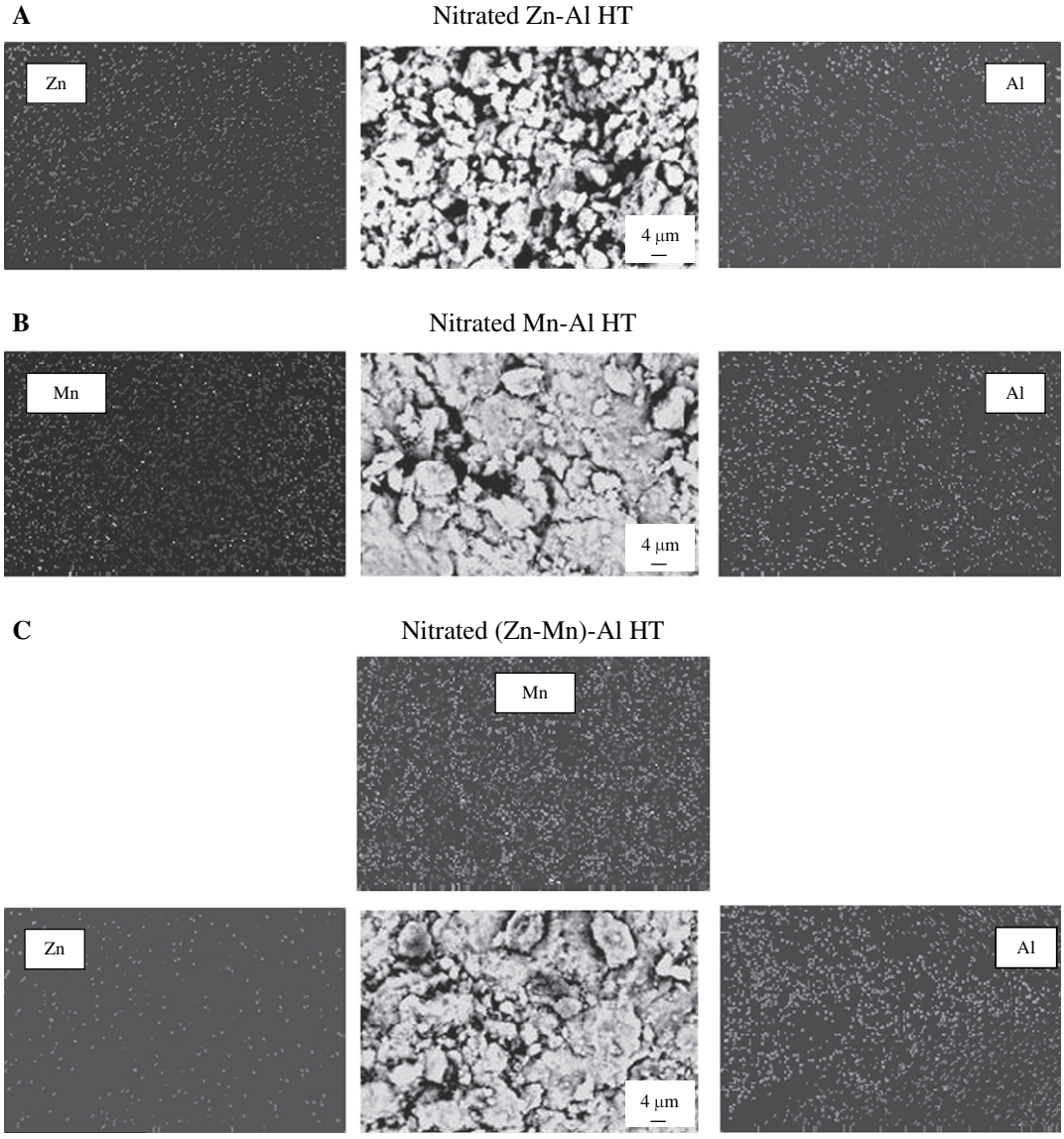

Fig. 3. EDX mapping of Zn, Mn and Al elements in nitrated HTs.

In the same way, the ternary (Zn-Mn)-Al HT shows a diffraction pattern indicating the Mn_2O_4 and $(Zn,Al)Mn_2O_4$ oxide formation. In the samples calcined at 723 K, Fig. 8, the same oxide species are formed with similar XRD peak intensities as those in the sample treated at 523 K. The oxide species are usually formed at a higher temperature, although our results may be compared with those of Kooli et al. [19] who report mixed oxides after calcinations at 573 K. This phenomenon has not been observed in the classical carbonated Mg–Al hydrotalcites, where no oxides are detected by XRD prior 773 K [20,21].

X-ray thermo-diffraction patterns display the evolution of Zn–Al HT with temperature *in situ*, Fig. 9. The brucite-like layered structure is preserved up to 438 K with an evident peak shift (003) towards larger angles 2θ showing that the interlayer space diminishes with dehydration. At 473 K the layered structure collapses and ZnO is formed. The Mn–Al and (Zn-Mn)-Al HT present a similar behaviour, but the layered structures collapse at 438 K and the peak intensities are lower than in Zn–Al HT.

3.2.2. N_2 physisorption

The BET surface area of the binary sample Zn–Al HT ($2\ m^2\ g^{-1}$) pretreated at 473 K is much smaller than those of Mn–Al and (Zn-Mn)-Al HTs (64 and $50\ m^2\ g^{-1}$, respectively), Table 3. The total pore volume shows a similar trend. The isotherm profiles of the Mn containing samples, Fig. 10, are Type II according to IUPAC [22].

At 523 K, the BET surface areas for Mn–Al and (Zn-Mn)-Al samples, 66 and $47\ m^2\ g^{-1}$, are similar to those of the dried samples, while for Zn–Al the surface area is larger, $19\ m^2\ g^{-1}$ (Table 3). Furthermore, the total pore volume increases $0.03\ cm^3\ g^{-1}$ in all samples. At 723 K, the three samples have similar BET surface areas, close to $70\ m^2\ g^{-1}$, and similar volumes (*ca.* $0.13\ cm^3\ g^{-1}$).

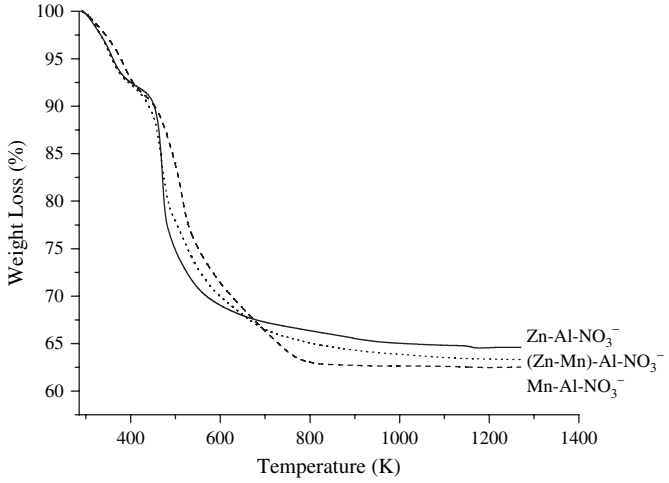

Fig. 4. TGA-N_2 behaviour of nitrated HTs.

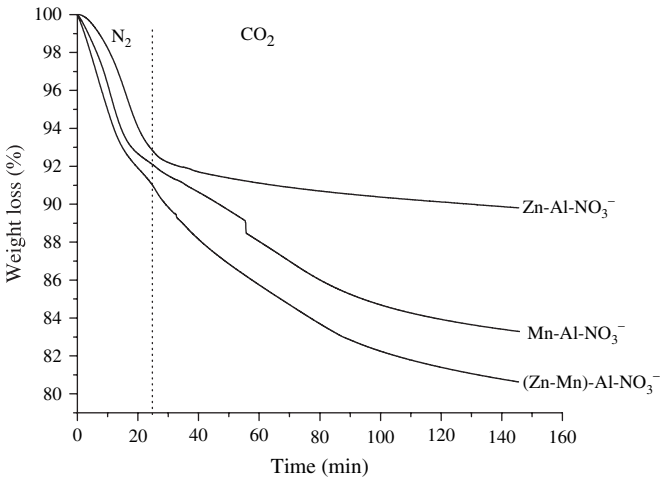

Fig. 6. Isothermal TGA-CO_2 (423 K) for nitrated HTs.

3.3. Permanganate intercalated HT samples

3.3.1. X-ray diffraction

The XRD patterns of the exchanged samples present broad peaks, Fig. 11. The diffractogram of the MnO_4^- exchanged Zn−Al sample corresponds to a nitrated hydrotalcite structure, $2\theta = 11.0° \pm 0.1$ ($d_{003} = 8.08$ Å) (shoulder) and $22.0° \pm 0.1$ ($d_{006} = 4.04$ Å). It also presents a first small peak at 9.0° ($d_{003} = 9.82$ Å) which may be compared with the peak position of the HT intercalated with MnO_4^- ($d_{003} = 8.80$ Å) [13]. The interlayer space produced by the intercalation is larger than the space required to homogeneously exchange permanganates. The second peak is found at 14.0° ($d_{006} = 6.32$ Å). Such distance is much higher than the expected in a permanganate intercalated hydrotalcite. It seems that a staged intercalation occurs [23]. This model consists of islands of intercalated anions located in distorted regions of the host diffusing towards the crystallite centre. This phenomenon is thought to be a consequence of the flexible nature of the brucite-like sheets.

Both Mn containing samples only present d_{003} distances at 12° ($d_{003} = 7.37$ Å). In these materials, the interlayered anion could be OH^- which as reported by Miyata [8] generates an interlayer distance of 7.55 Å. The small d_{003} difference has to be attributed to the heterogeneous distribution of the anions, revealed by the broadness of the X-ray diffraction peaks, although this sample is rather complex as the second X-ray diffraction peak is not harmonic with the first. Note that the (012) and (110) peaks of the Mn intercalated samples are clearly shifted towards larger angles. These reflections depend on the layer structure (cell parameters a and b), therefore the brucite layer geometry is altered by the strong interaction with the pillars.

If MnO_4^- and water were incorporated in Zn−Al HT after the calcination step at 523 K, no regeneration was observed as shown by XRD, Fig. 12: the initial Zn oxides remained. In contrast, for comparison purposes, only in the presence of Na_2CO_3, highly crystalline carbonated Zn−Al HT was partially formed, Fig. 12. In the same way, the HTs containing Mn did not reconstruct through memory effect, Figs. 13 and 14, in the presence

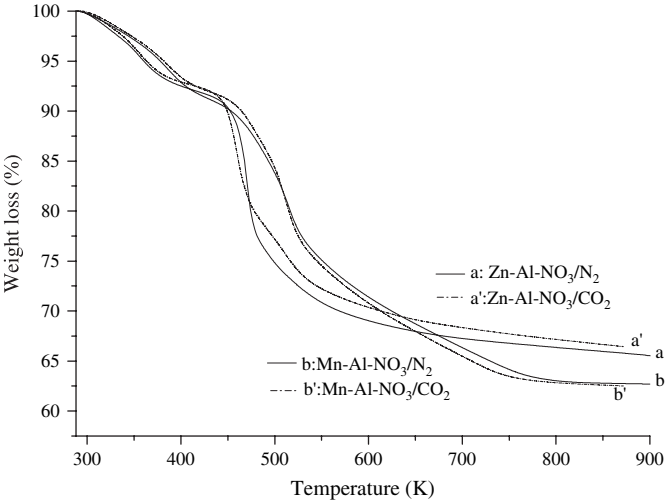

Fig. 5. TGA-CO_2 and N_2 profiles for nitrated Zn−Al and Mn−Al HTs.

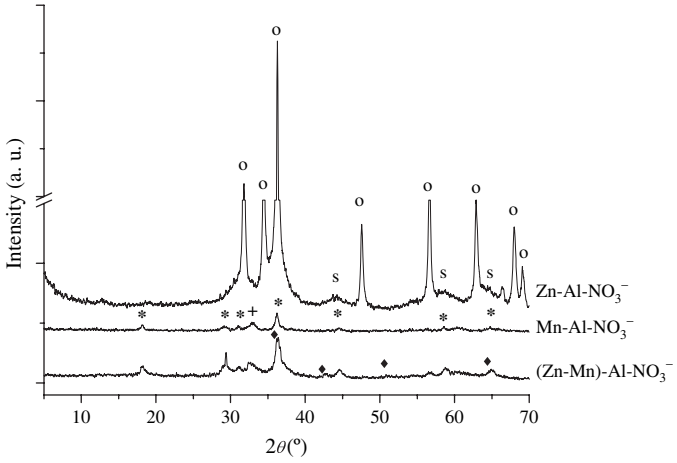

Fig. 7. XRD patterns of nitrated HTs calcined at 523 K. (∗) Mn_2O_4, (+) Mn_2O_3, (◆) (Zn,Al)Mn_2O_4, (o) ZnO, (s) $ZnAl_2O_4$.

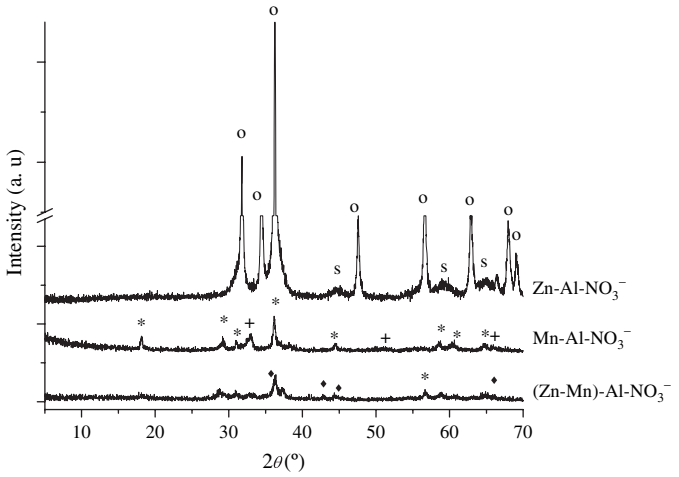

Fig. 8. XRD patterns of nitrated (Zn,Mn)-Al HTs calcined at 723 K. (∗) Mn_2O_4, (+) Mn_2O_3, (◆) (Zn,Al)Mn_2O_4, (o) ZnO, (s) $ZnAl_2O_4$.

of MnO_4^- or water. Moreover, the calcined samples at 523 K were not regenerated in the presence of CO_3^{2-}.

3.3.2. N_2 physisorption

After incorporation of MnO_4^- by ion exchange, the surface areas increased considerably, 116–181 $m^2\,g^{-1}$, Table 3. The total pore volume increased as well in all samples, 0.53–0.66 $cm^3\,g^{-1}$. These results are in agreement with the XRD patterns, because the broad peaks indicate that the mean particle size decreases and this obviously accounts for the increase of surface area.

3.3.3. FTIR spectroscopy

The FTIR spectra for the NO_3^- and MnO_4^- hydrotalcites are compared in Fig. 15. All spectra present a broad adsorption band at 3450 cm^{-1} attributed to the stretching vibration of the hydroxyl group (OH) from the hydroxide layers and

Table 3
Physisorption properties of HTs, on the one hand, dried at 343 K, calcined at 523 and 723 K and, on the other, MnO_4^- exchanged (dried at 343 K)

NO_3^--HT	BET ($m^2\,g^{-1}$)				Total pore volume ($cm^3\,g^{-1}$)			
	Temperature (K)			MnO_4^- incorporated by exchange	Temperature (K)			MnO_4^- incorporated by exchange
	343	523	723		343	523	723	
Zn–Al	2	19	70	121	<0.01	0.04	0.12	0.66
Mn–Al	64	66	71	181	0.07	0.11	0.13	0.58
(Zn-Mn)-Al	50	47	64	116	0.07	0.10	0.14	0.53

the interlayer water. The broadening of this band is caused by the hydrogen bond formation [1,13]. The band close to 1640 cm^{-1} corresponds to a deformation mode of H_2O molecules. In Fig. 15 the spectra were normalized to the water band at 1639 cm^{-1}. Indeed, the samples were not diluted and the TGA experiments showed that the amount of water was similar in all samples. The band of OH vibration diminishes after ion intercalation in the samples containing Mn. In consequence, partial dehydroxylation during the exchange step can occur. The intense bands at 1394 and 1344 cm^{-1} are consistent with the ν_3 mode of nitrate and carbonate species, respectively. The very small broad band vibration at 1030 cm^{-1} is observed only for Mn–Al and (Zn-Mn)-Al nitrated samples and it is attributed to the symmetric valence vibration of carbonate [24]. Only the MnO_4^- incorporated Zn–Al sample presents a band at 1201 cm^{-1} which has to be caused by the MnO_4^- anions.

In the MnO_4^- incorporated samples, the ν_3 vibration of NO_3^- diminishes, and a band at 960 cm^{-1} for Zn–Al–MnO_4 sample appears, but in MnO_4^- incorporated Mn–Al and (Zn-Mn)-Al samples this band shifts to 902 cm^{-1}. It is attributed to the antisymmetric stretching vibration ν_3 of the tetrahedral MnO_4^-. These results show that MnO_4^- anions interact with the OH^- in the layered structure. Bands observed below 800 cm^{-1} are due to the vibration of the metal–oxygen bonds in the brucite-like sheets.

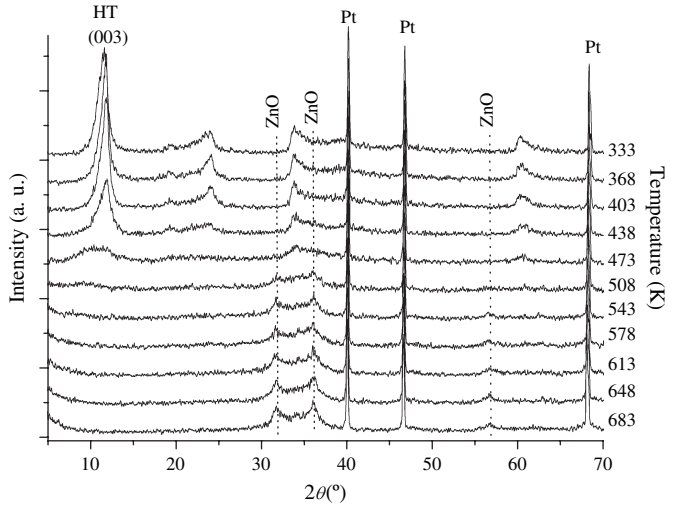

Fig. 9. X-ray thermo-diffraction patterns of nitrated Zn–Al HT from 333 to 683 K ($\Delta T = 35$ K). Peaks corresponding to Pt are due to sample holder.

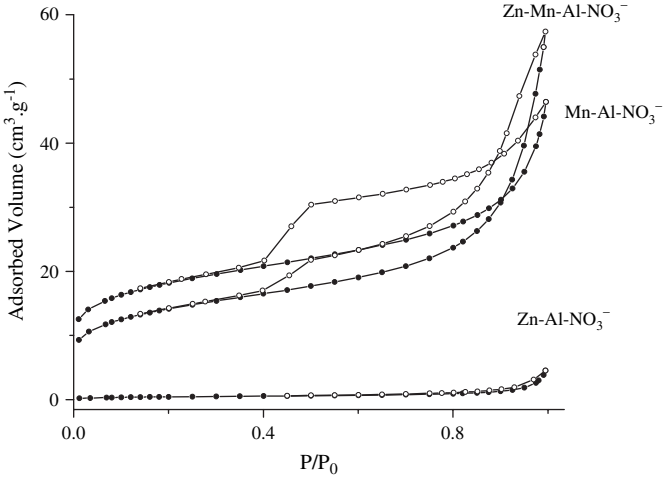

Fig. 10. N_2 adsorption–desorption isotherms of dried NO_3^--HTs (adsorption branch: black circles, desorption branch: empty circles).

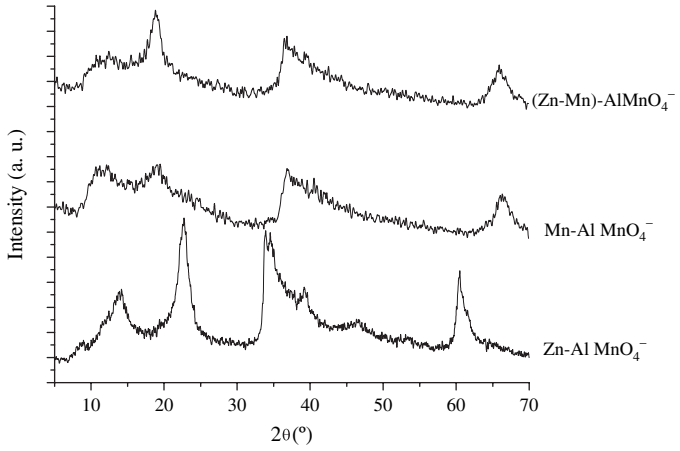

Fig. 11. XRD patterns of MnO_4^- HTs dried at 343 K.

3.3.4. CO_2 sorption

The thermal behaviour of the MnO_4^- incorporated samples in the presence of N_2 and CO_2 was similar to the nitrated samples. No CO_2 or carbonates were retained (data not shown).

4. Discussion

The previous results show that binary and ternary nitrated hydrotalcites may be synthesized with Zn^{2+} and Mn^{2+} in the presence of microwave irradiation. The obtained materials are comparable with those reported in Refs. [16,25]. If MnO_4^- anions are incorporated, through HT regeneration, they are not intercalated; instead, if the method followed is the anion exchange, the HTs may be, in some cases, partially intercalated. XRD results are in agreement with those from BET as the surface area is large and XRD shows partial crystallization of layered materials. BET surface areas are similar to those reported by Villegas et al. [15] for permanganated Mg−Al HTs. Furthermore, FTIR spectroscopy indicates that MnO_4^- anions interact with the OH^- of brucite-like sheets. Although, in our preparations, crystallinity is low, it could be due to partial reduction of MnO_4^- to MnO_x species during microwave irradiation, as temperature in the reactor reaches 353 K.

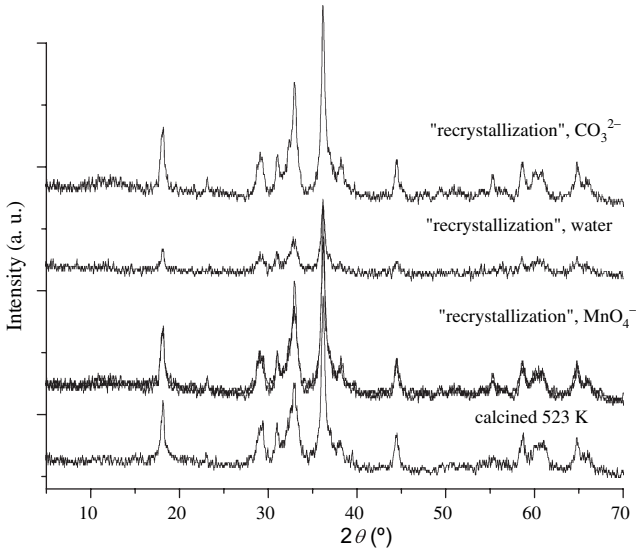

Fig. 13. XRD patterns of Mn−Al nitrated HT calcined at 523 K and ''recrystallized'' through the incorporation of either MnO_4^-, water or CO_3^{2-}.

Our TGA results show that no CO_2 is retained in our samples, either as CO_2 or as carbonates. In other words, there is no physisorption or chemisorption. This phenomenon may be caused by a sterical effect as interlayered NO_3^- anions could hinder the CO_2 sorption. However, at 423 K, nitrated HTs present an interlayer space large enough to allow CO_2 diffusion [1]. Hence, no steric effects inhibit the access of CO_2 to exchange sites. Moreover, diffusing CO_2 could react to produce carbonates. CO_2 may enter the interlayer space of the nitrated HTs as discussed previously and it could react with the water already present between the layers to form CO_3^{2-}. Again, as no retention is observed this mechanism has to be

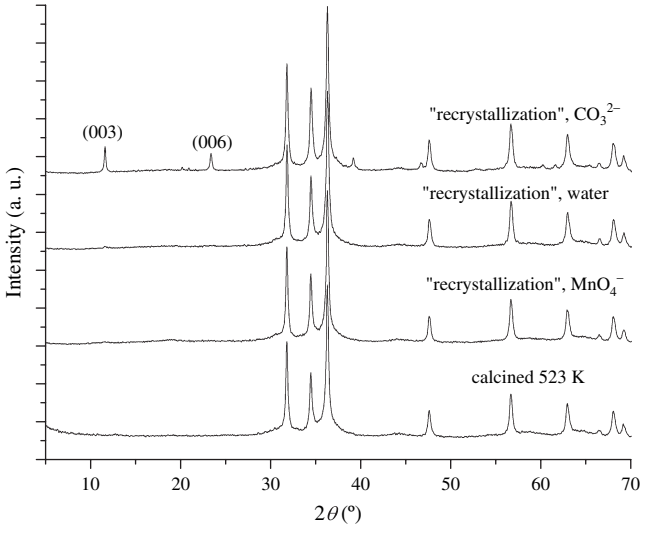

Fig. 12. XRD patterns of Zn−Al nitrated HT calcined at 523 K and ''recrystallized'' through the incorporation of either MnO_4^-, water or CO_3^{2-}.

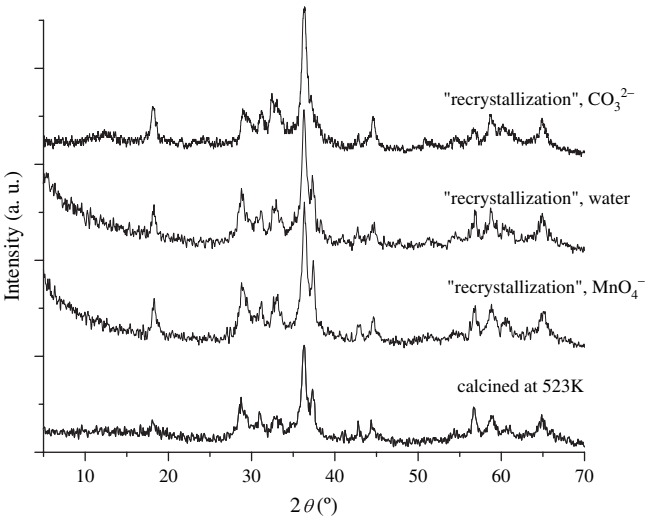

Fig. 14. XRD patterns of (Zn,Mn)-Al nitrated HT calcined at 523 K and ''recrystallized'' through the incorporation of either MnO_4^-, water or CO_3^{2-}.

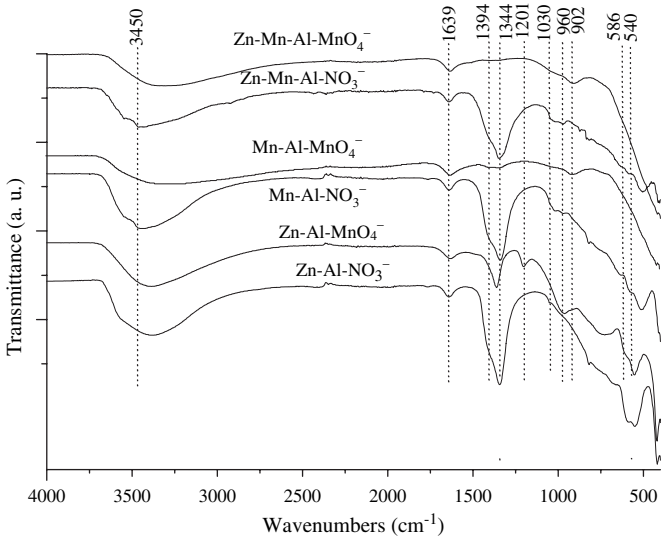

Fig. 15. FTIR spectra of NO_3^- and MnO_4^- HTs.

discarded. Furthermore, calcined samples (523 K) did not reconstruct from CO_3^{2-}, only the Zn−Al HT presents a partial regeneration in extreme conditions.

The sorption of CO_2 at 423 and 473 K in Mg−Al HTs has been reported by Moreira et al. [26]; they have explained the sorption capacity variation with temperature through entropic effects. However, our samples are carbonate phobic hence this proposition cannot be considered. The carbonate phobic properties may be correlated with the basic and electronegative features of the metal layered hydroxides. In simple oxides the basic character is determined by the metal electronegativity [27] and, in hydrotalcites, it depends on the metal layered electronegativities. The basic properties are determined by the M^{2+} cations. Furthermore, the charge density in the layer affects the interactions between anions and the metal cations.

Sanderson [28] has reviewed the electronegativity character of all the active major group elements and he has proposed the following principle of electronegativity equalization: "When two or more atoms initially different in electronegativity combine, they become adjusted to the same electronegativity within the compound" [29]. This principle has been applied by Camacho-Rodrigues [30] to understand the effect of the composition on the electronegativities of binary HTs. In our work, the difference between layered M^{2+} electronegativities, zinc and manganese, can diminish the basic character of nitrated (Zn,Mn)-Al HTs, if compared to the classical carbonated Mg−Al hydrotalcite. The binary Zn^{2+}−Al and Mn^{2+}−Al HTs present electronegativity values of 3.01 and 2.73, respectively; they are both higher than Mg^{2+}−Al HT (2.50). In conventional Mg−Al HT, the electron transfer is from Mg (1.32) to Al (1.74) *via* an oxygen bridge, but, in nitrated Zn−Al HT, it is from Al to Zn (2.22). However, the nitrated Mn−Al HT could present an electron transfer from Mn (1.66) to Al (1.74), though electronegativity values are very close. The nitrated HTs containing Zn or Mn present, then, layers with an electropositive character lower than those of carbonated Mg−Al HT. In consequence, the basicity of oxygen, as well as the acidity of metal centres are strongly modified and the replacement of Mg^{2+} by Zn^{2+} or Mn^{2+} leads to poor interactions between M^{2+} and carbonate molecules. Thus, the sorption of CO_2 is not favoured.

These phobic properties can be better understood if we consider that local electronegativity (or basicity) is linked to the coordination number of M^{2+} atoms with oxygen [30]. Local electronegativity in HT has been also defined by Camacho-Rodrigues [30]; this concept predicts that the difference between local and average composition affects the basicity of oxygen atoms. Fig. 16 shows, for some binary M^{2+}−Al HTs, that increasing surrounding M^{2+} atoms does not increase the basicity in all of them. Indeed, HTs containing Cr^{2+} and Mg^{2+} are the most basic compounds. In contrast, the basicity in the HTs containing Co^{2+} and Zn^{2+} is lower. In our HTs the nominal M^{2+}/Al^{3+} molar ratio was 2/1 for all samples, but some oxide species are formed with HTs containing Mn^{2+}, as previously reported. Mn oxides present a poor basicity since the number of surrounding M^{2+} atoms must be close to 6 (Fig. 16). Furthermore, Mn compounds present different oxidation states: II, III, IV, V and VI; with an increase of their Sanderson electronegativities: 1.66, 2.20, 2.74, 3.28 and 3.82, respectively.

If the correlation between basicity and Sanderson electronegativities is accepted, results previously reported in the bibliography may be understood. Sanchez-Valente et al. [31] have studied nitrated and chlorided HTs. Their calcined hydrotalcite containing Cu^{2+} (electronegativity = 1.98) presents a poor CO_2 sorption, *ca.* 0.095 meq $CO_2\,g^{-1}$. In this material again, the electron transfer is from Al to Cu. In contrast, the Ni−Al HT presents CO_2 sorption much higher.

Still, such correlation fails if nickel is present. The highest concentration of basic sites was observed for a carbonated Mg−Ni−Al HT with low magnesium and high nickel content (0.33/1.67/1) [32]. Although, Sanderson electronegativity of Ni^{2+} (1.94) is almost the same as Cu^{2+} (1.98), the electron transfer prevails between Mg and Al. In this report, a synergetic effect is proposed between the two M^{2+} cations, which modify the basic properties.

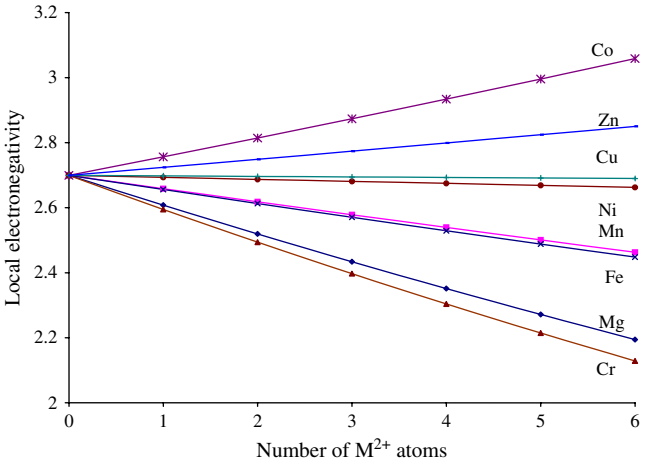

Fig. 16. Influence of surrounding M^{2+} atoms on electronegativity (or basicity) in binary M^{2+}−Al HTs.

In hydrotalcites with different interlayered anions, Zhang et al. [33] have observed that the basicity of a $Cu^{2+}/Ni^{2+}/Cr^{3+}$ calcined sample with a molar ratio of 1/2/1 increases in the following order: HT-CO_3^{2-} > HT-NO_3^- > HT-SO_4^{2-}. In the same way, Kustrowski et al. [34] have reported that a carbonated Mg–Al HT presents basic sites much stronger than sulfated and nitrated Mg–Al hydrotalcites.

5. Conclusions

Nitrated hydrotalcites with Zn or/and Mn as M^{2+} and Al as M^{3+} were synthesized in the presence of microwave irradiation. If MnO_4^- anions were incorporated *via* memory effect, the hydrotalcites did not crystallize. If the method followed was the anion exchange, the hydrotalcites were partially intercalated. These materials present carbonate phobic properties which were correlated with the basic and electronegative features of the brucite-like layers. The nitrated or permanganated HTs containing Zn or Mn layers presented a poorer basicity than Mg–Al HTs. Therefore, the sorption of CO_2 is not favoured, nor the formation of carbonates. Due to carbonate phobic properties, these materials may be used as adsorbents in different processes in the presence of carbonate environment.

Acknowledgements

This work was financially supported by the projects IN103506 PAPIIT-UNAM and 44253-Q CONACYT. Authors thank J. Guzmán and L. Baños for their technical work in the SEM and XRD analyses, respectively. We thank also C. Vázquez and E. Fregoso for the TGA experiments.

References

[1] F. Cavani, F. Trifiro, A. Vaccari, Catal. Today 11 (1991) 173.
[2] D.G. Evans, R.C.T. Slade, Struct. Bonding 119 (2006) 1.
[3] F. Li, X. Duan, Struct. Bonding 119 (2006) 193.
[4] V. Rives, M.A. Ulibarri, Coord. Chem. Rev. 181 (1999) 61.
[5] F. Trifirò, A. Vaccari, in: J.L. Atwood, J.E.D. Davies, D.D. MacNicol (Eds.), Comprehensive Supramolecular Chemistry, vol. 7, Pergamon, Kidlington, Oxford, 1996, p. 251.
[6] A. Vaccari, Catal. Today 41 (1998) 53.
[7] J.A. Rivera, G. Fetter, P. Bosch, Microporous Mesoporous Mater. 89 (2006) 306.
[8] S. Miyata, Clays Clay Miner. 31 (1983) 305.
[9] Z. Yong, V.G. Mata, A.E. Rodrigues, Ind. Eng. Chem. Res. 40 (2001) 204.
[10] M.T. Olguin, P. Bosch, D. Acosta, S. Bulbulian, Clays Clay Miner. 46 (1998) 567.
[11] S. Velu, V. Ramaswamy, S. Sivasanker, Chem. Commun. (1997) 2107.
[12] A.V. Radha, P. Vishnu-Kamath, Bull. Mater. Sci. 26 (2003) 661.
[13] T. Kühn, H. Pöllman, in: M. Pecchio, F.R. Días de Andrade (Eds.), 8th International Congress on Applied Mineralogy, Aguas de Lindoia, Sao Paulo, Brasil, 2004.
[14] J.T. Kloprogge, L. Hickey, R.L. Frost, J. Solid State Chem. 177 (2004) 4047.
[15] J.C. Villegas, O.H. Giraldo, K. Laubernds, S.L. Suib, Inorg. Chem. 42 (2003) 5621.
[16] S. Aisawa, H. Hirahara, H. Uchiyama, S. Takahashi, E. Narita, J. Solid State Chem. 167 (2002) 152.
[17] P. Beaudot, M.E. De Roy, J.P. Besse, Chem. Mater. 16 (2004) 935.
[18] M. Del Arco, S. Gutiérrez, C. Martín, V. Rives, Inorg. Chem. 42 (2003) 4232.
[19] F. Kooli, K. Kosuge, A. Tsunashima, J. Solid State Chem. 118 (1995) 285.
[20] S. Miyata, Clays Clay Miner. 28 (1980) 50.
[21] T. Sato, T. Wakabayashi, M. Shimada, Ind. Eng. Chem. Prod. Res. Dev. 25 (1986) 89.
[22] F. Rouquerol, J. Rouquerol, K.W. Sing, in: F. Schüth, K.S.W. Sing, J. Weitkamp (Eds.), Handbook of Porous Solids, vol. 1, Wiley-VCH, Weinheim, Germany, 2002.
[23] A.M. Fogg, J.S. Dunn, D. O'hare, Chem. Mater. 10 (1998) 356.
[24] S. Kannan, C.S. Swamy, J. Mater. Sci. 32 (1997) 1623.
[25] A. Chen, H. Xu, Y. Yue, W. Shen, W. Hua, Z. Gao, Ind. Eng. Chem. Res. 43 (2004) 6409.
[26] R. Moreira, J. L Soares, G.L. Casarin, A.E. Rodrigues, Sep. Sci. Technol. 41 (2006) 341.
[27] K.I. Tanaka, A. Ozaki, J. Catal. 8 (1967) 1.
[28] R.T. Sanderson, J. Am. Chem. Soc. 105 (1983) 2259.
[29] R.T. Sanderson, Inorg. Chem. 25 (1986) 3518.
[30] A.C. Camacho-Rodrigues, J. Math. Chem. 37 (2005) 347.
[31] J. Sanchez-Valente, F. Figueras, M. Gravelle, P. Kumbhar, J. Lopez, J.P. Besse, J. Catal. 189 (2000) 370.
[32] S. Casenave, H. Martinez, C. Guimon, A. Auroux, V. Hulea, A. Cordoneanu, E. Dumitriu, Thermochim. Acta 379 (2001) 85.
[33] L. Zhang, J. Zhu, X. Jiang, D.G. Evans, F. Li, J. Phys. Chem. Solids 67 (2006) 1678.
[34] P. Kustrowski, L. Chmielarz, E. Bozek, M. Sawalha, F. Roessner, Mater. Res. Bull. 39 (2004) 2631.